DOI: 10.1002/marc.((insert number))

Communication

Self-assembly of diblock molecular polymer brushes in the spherical confinement of nanoemulsion droplets[a]

Andrea Steinhaus,[±] Théophile Pelras,[±] Ramzi Chakroun, André H. Gröschel,[*] Markus Müllner[*]

[±]The authors contributed equally.
A. Steinhaus (M.Sc.), R. Chakroun (M.Sc.), Prof. Dr. A.H. Gröschel
Physical Chemistry and Center for Nanointegration Duisburg-Essen (CENIDE), University Duisburg-Essen, 47057 Duisburg, Germany.
E-mail: andre.groeschel@ude.de
T. Pelras (M.Sc.), Dr M. Müllner
Key Centre for Polymers and Colloids, School of Chemistry, and The University of Sydney Nano Institute (Sydney Nano), The University of Sydney, Sydney 2006, New South Wales, Australia.
E-mail: markus.muellner@sydney.edu.au

Abstract: Understanding the self-assembly behavior of polymers of various topologies is key to a reliable design of functional polymer materials. Self-assembly under confinement conditions emerges as a versatile avenue to design polymer particles with complex internal morphologies while simultaneously facilitating scale-up. However, only linear block copolymers have been studied to date, despite the increasing control over macromolecule composition and architecture available. This study extends the investigation of polymer self-assembly in confinement from regular diblock copolymers to diblock molecular polymer brushes (MPBs). Block-type MPBs with polystyrene (PS) and polylactide (PLA) compartments of different sizes are incorporated into surfactant-stabilised oil-in-water (chloroform/water) emulsions. The increasing confinement in the nanoemulsion droplets during solvent

[a] **Supporting Information** is available online from the Wiley Online Library or from the authors.

evaporation directs the MPBs to form solid nano/microparticles. Microscopy studies reveal an intricate internal particle structure, including interpenetrating networks and axially-stacked lamellae of PS and PLA, depending on the PS/PLA ratio of the brushes.

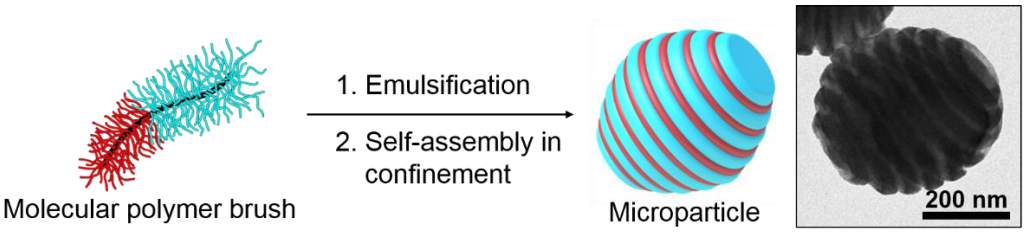

1. Introduction

The equilibrium self-assembly of block copolymers in bulk and dilute solution has been thoroughly studied in the last two decades,[1, 2] focusing predominately on the investigation of the structure formation of diblock copolymers. Numerous self-assembly approaches have been developed to achieve intricate nanostructures, including the use of polymer blends, multiblock copolymers, and different polymer topologies.[3] Research on more complex copolymers has meanwhile progressed the field towards innovative nanomaterials featuring surface pattern, inner structure, and complex chemical composition.[4] The formation of nano- and microparticles *via* a more direct route remains an area of focused research effort, where block copolymer self-assembly in confinement (*i.e.* under the influence of high-energy, structure-directing interfaces) emerges as particularly versatile in the formation of structured nanomaterials.[5-7] Polymer microphase separation in the spherical confinement of nanoemulsion droplets combines the scalability of emulsions with the versatility of structure control through droplet size (and in turn curvature).[8] Recent studies, using regular diblock copolymers of varied block lengths, developed a fundamental understanding of the effects of curvature,[9] evaporation rate,[10] surfactants and particle/polymer postmodification.[11-16] Only few studies have focused on more complex copolymers, such as ABC triblock terpolymers.[17, 18] So far, there have been no reports on the self-assembly of polymer architectures (such as molecular polymer brushes, MPBs) within the confinement of emulsion droplets, despite distinctly and unique properties in comparison to their linear analogues. However, the use of MPBs in the production of functional polymer materials has been rapidly increasing in recent years.[19, 20]

MPBs (or polymer bottlebrushes) are a class of soft materials with unique properties that arise from its architecture.[21, 22] They consist of a polymer backbone that is grafted with polymer side chains – typically leading to a stretched conformation of side chains and backbone. As

MPBs show minimised chain entanglement, they are being increasingly investigated for self-assembly applications and their behavior at interfaces.[23, 24] In particular, diblock MPBs comprise already phase-separated compartments of high molecular weight and different chemistry which renders such block- or Janus-type MPBs into nanoscale building blocks suitable for assembly in solution and bulk. Owing their distinct brush architecture, MPBs have shown faster phase separation than their linear analogues.[25] Similarly, molecular brushes have featured in several self-assembly studies (in bulk, melt and thin films) where the morphology can be tuned *via* brush length, composition, shape and/or grafting density – yielding, for example, lamellae with tunable domain spacings[26-28] or cylindrical domains that can be transformed into nanopores.[29]

Here we studied the self-assembly of MPBs in the spherical confinement of nanoemulsion droplets. An increasing spherical confinement during solvent evaporation directed MPBs comprising of polystyrene (PS) and polylactide (PLA) to form solid nano/microparticles with intricate internal morphologies. As a proof-of-concept, we investigated the particle formation and analysed the effects of PS/PLA ratio on the microparticle structure using a combination of electron microscopy and tomography.

2. Results and Discussion

The MPBs were synthesised using the 'grafting-from' approach (**Scheme 1**a). Starting with the formation of a symmetric backbone capable of initiating separate grafting steps, we used reversible addition-fragmentation chain-transfer (RAFT) polymerisation to produce poly[2-(2-bromoisobutyryloxy)ethyl methacrylate]-*block*-poly[2-(trimethylsilyloxy)ethyl methacrylate], namely $PBIEM_{92}$-*b*-$P(TMS\text{-}HEMA)_{104}$. Deprotection of the TMS group freed the hydroxyl functions yielding $PBIEM_{92}$-*b*-$PHEMA_{104}$ – a backbone that can be grafted by both atom transfer radical polymerisation (ATRP) and ring opening polymerisation (ROP). A diblock brush architecture was achieved by sequential grafting-from steps, starting with the grafting of

polylactide side chains onto PHEMA *via* a organo-catalysed ROP. Subsequent grafting from PBIEM added a polystyrene compartment (with control over side chain length) to yield diblock MPBs [PBIEM$_{92}$-*g*-PS$_x$]-*b*-[PHEMA$_{104}$-*g*-PLA$_{33}$] (x = 6 or 24). The individual synthesis steps can be found in the Supporting Information (Figure S1). Atomic force microscopy (AFM) revealed discrete single brush entities (Figure S2) of similar dimensions.

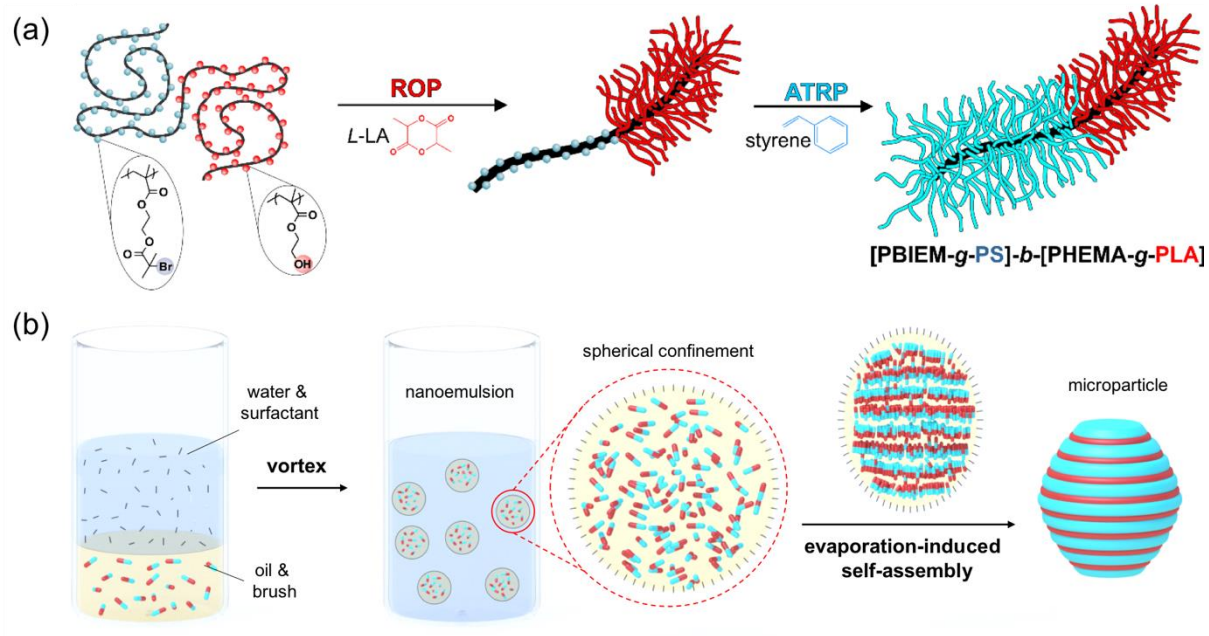

Scheme 1. Synthesis and self-assembly of diblock molecular polymer brushes in the confinement of nanoemulsion droplets. (a) Step-wise synthesis of [PBIEM$_{92}$-*g*-PS$_x$]-*b*-[PHEMA$_{104}$-*g*-PLA$_{33}$] from PBIEM$_{92}$-*b*-PHEMA$_{104}$ polyinitiator. (b) Preparation steps to form microparticles from $CHCl_3$/water emulsions by evaporation-induced self-assembly of the MPBs.

To prepare microparticles, we dispersed the diblock MPBs (c = 6.67 g·L^{-1}) in $CHCl_3$ – a good solvent for all blocks that is immiscible with water and evaporates quickly (Scheme 1b). The MPB dispersion was mixed with water containing a surfactant (c = 10 g·L^{-1}) and vortexed for 1 min to form a nanoemulsion. Through the controlled evaporation of $CHCl_3$, the emulsion droplet size continuously reduced which in turn increased the concentration of brushes within.

At a critical concentration, the MPBs microphase separated into morphologies specific to the volume fraction of the brush compartments. The final brush morphology is additionally affected by the high energy boundary of the curved droplet/water interface during drying, which may result in unusual morphologies differing from those observed under equilibrium bulk conditions.

Using the above described process, we first prepared microparticles from [PBIEM$_{92}$-*g*-PS$_6$]-*b*-[PHEMA$_{104}$-*g*-PLA$_{33}$] (**MPB1**; f_{PS} ~ 20 wt%) (**Figure 1**). The surfactant may cause preferential orientation of polymer blocks towards the interface and hence define the shape of the microparticles. We therefore first compared three different surfactants namely sodium dodecyl sulfate (SDS), cetyltrimethylammonium bromide (CTAB), and polyvinyl alcohol (PVA). Stable dispersions and the absence of macroscopic precipitation verified the effectiveness of all three surfactants (Figure 1a). DLS shows comparable hydrodynamic radii of $R_{h,\,CTAB}$ = 168 nm, $R_{h,\,PVA}$ = 186 nm, $R_{h,\,SDS}$ = 131 nm with surprisingly narrow size distributions for CTAB and SDS (Figure 1b). However, TEM highlighted CTAB as the best suited candidate to prepare uniform microphases (Figure S3), which we then used as the surfactant-of-choice throughout the rest of the study.

To gain detailed information of the particle morphology, we analysed the CTAB-stabilised microparticles in TEM using RuO_4 staining to enhance the contrast of the PS domain (while the PLA domain appears bright) (Figure 1c). TEM revealed well-developed particles with overall spherical shape (~200-500 nm in diameter) and a rather complex inner structure resembling a bi-continuous interpenetrating network. The development of such a bi-continuous (or gyroid-like) morphology is typically found by diblock copolymers with specific asymmetric block ratio,[30] if classic theory of microphase separation of block copolymers is applied. Our brushes had a ratio of 20:80 of the PS/PLA fractions, a ratio which would generally be associated with cylindrical morphologies in case of linear block copolymers.[31] We will discuss the network

structure in more detail below. The microparticles displayed a corrugated surface with *fuzzy* appearance, which most likely originates from the bi-continuous morphology as well as the high contour length of MPBs (as compared to coiled polymer chains). In SEM, we observed a wrinkled surface structure/topography presumably caused by selective beam damage or particle shrinking after sputtering (Figure 1d). The inner structure of the PS network supports anisotropic shrinking resulting in the characteristic wrinkling pattern (the PS scaffold remains largely intact). However, it is still surprising that the particles seem to be engulfed in a continuous polymer layer, which will be investigated further in future.

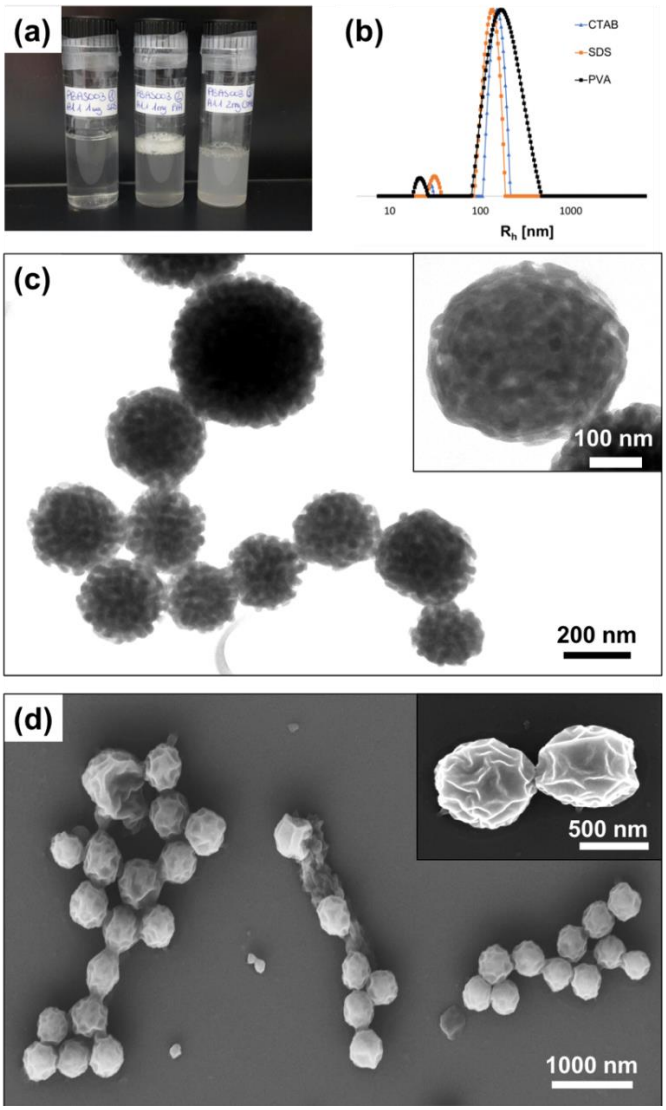

Figure 1. Microparticles made from [PBIEM$_{92}$-*g*-PS$_6$]-*b*-[PHEMA$_{104}$-*g*-PLA$_{33}$] (c_{MPB1} = 6.67 g·L^{-1}). (a) Photographic series showing surfactant-stabilised dispersions: (a)

surfactant concentration was 10 $g \cdot L^{-1}$; i) SDS, ii) CTAB, and iii) PVA. (b) DLS of particle size distribution of the solutions shown in (a). (c) TEM overview image of inner structure (RuO_4 stained); inset highlighting the interpenetrating network. (d) SEM overview image of CTAB-stabilised microparticles; inset illustrates shape and surface structure on magnified particles.

To further study the internal features, we investigated individual particles *via* TEM tomography (**Figure 2**). Collecting tilt series on a single particle (Figure 2a and Supporting Video 1), we calculated a three-dimensional (3D) reconstruction of the core structure (see SI for details). The electron density map of the reconstruction confirmed a bi-continuous network structure (Figure 2b), where the electron density increases from green to orange and is largely attributed to the PS domain. A zoom into the inside suggests an interconnected channel system of PLA ("empty" space) embedded in a PS matrix (green) (Figure 2c). The morphology lacks well-developed symmetry features which might be attributed to the comparably strong confinement conditions (D/L_0) for polymer brushes, *i.e.* a periodicity of ca. L_0 = 50 nm is confined to particles with D = 200-500 nm (D/L_0 = 4-10). Although a D/L_0 = 3-4 is typically considered weak confinement for polymer chains,[9] for stretched and more rigid brushes this does not seem to be the case. Determining the boundary conditions to define weak and strong confinement for other polymer topologies such as brushes are very relevant, but obviously require larger sample sets. According to classical phase behavior of diblock copolymers, the volume fraction of the brush, f_{PS} = 20 wt%, falls in the range of a cylindrical microphase observed between f_A = 20-40 wt% at low enthalpic repulsion. Refining the preparation conditions may yield larger particles with weaker confinement (e.g. $D/L_0 > 10$) where the inner structure more closely resembles the bulk case.

Since PLA can be degraded by acid hydrolysis, we subsequently etched the particles by adding 1M HCl to investigate the integrity of the particle structures (Figure 2d). After etching, the contrast between the PS and PLA phases has largely been enhanced (see also Figure S4) –

suggesting PLA removal. More importantly, individual particles remained intact, which further affirms that the PS domain is interconnected and aiding the particle integrity.

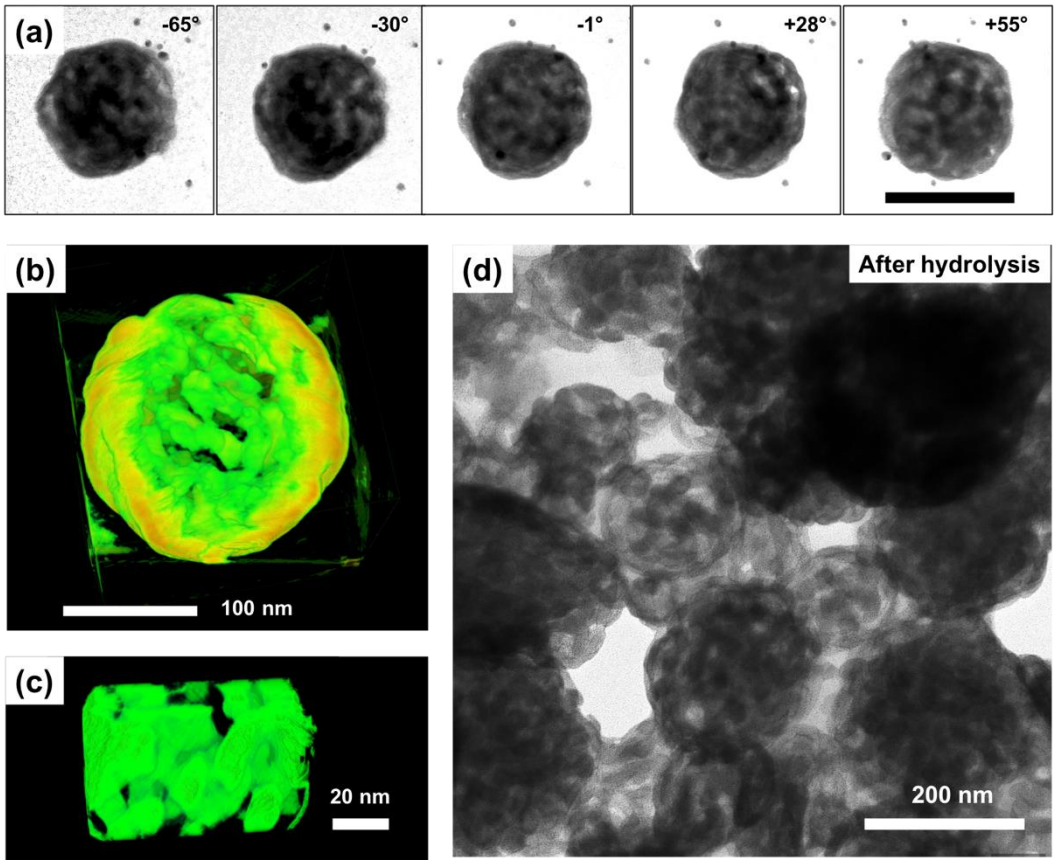

Figure 2. TEM tomography revealing the interpenetrating network of MPB1 microparticles. (a) Selected images from the tilt series of a single microparticle; tilt angles are as specified in the images. Scale bar is 200 nm. (b) Calculated electron density map of the entire particle after reconstruction (Gaussian volume filter applied). (c) Visualisation of the internal network structure only. (d) TEM overview of microparticles after acid treatment.

Next, we investigated the effect of a larger PS fraction using [PBIEM$_{92}$-*g*-PS$_{24}$]-*b*-[PHEMA$_{104}$-*g*-PLA$_{33}$] brushes (**MPB2**; f_{PS} ~ 55 wt%) with closely matching compartment sizes based on molecular weight. Contrary to the asymmetric MPB1, the particles of MPB2 showed a highly ordered, axially stacked lamellar morphology (**Figure 3**, Figure S5). The particles had a pronounced striped topography and were slightly elliptic with a size ranging from 300-1000 nm

(Figure 3a). We attributed the riffled surface to the alternating PS/PLA lamellae which can also be seen in TEM as highly contrasted, axially stacked layers (average thickness of $d \sim 40$ nm) – especially when the particles were found lying on the elliptic long axis (Figure 3b, Figure S6). Particles slightly tilted towards the viewing direction revealed a round, disk-like shape of individual lamellae, the stacking of which may also be responsible for stretching of the particle and its anisotropic shape.

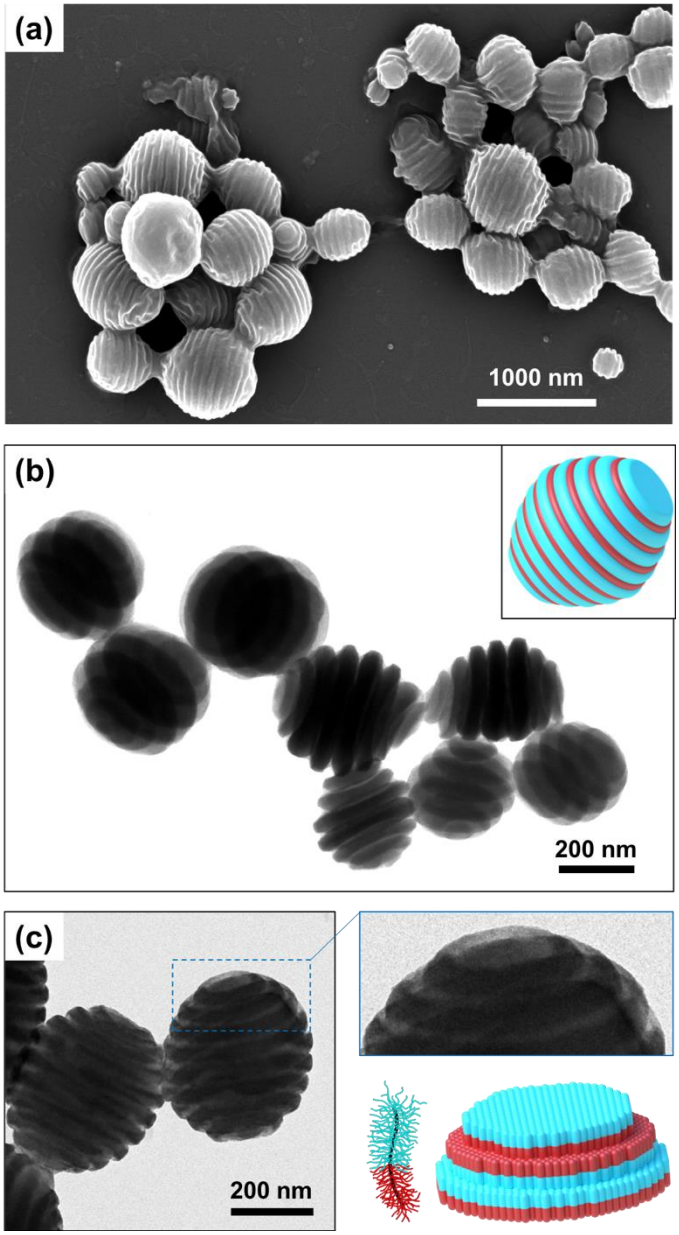

Figure 3. Axially-stacked lamellae of [PBIEM$_{92}$-*g*-PS$_{24}$]-*b*-[PHEMA$_{104}$-*g*-PLA$_{33}$] particles (c_{MPB2} = 6.67 g·L^{-1}, c_{CTAB} = 10 g·L^{-1}). (a) SEM image showing riffled surface structure

(topography). (b) RuO_4 stained TEM overview and (c) TEM close-up image revealing terrace-like lamella (axially stacked); Schematic clarifies the dense packing of the MPBs layers at the planar interfaces.

TEM drastically highlights a sharp interface boundary between PS (dark) and PLA (bright) domains (Figure 3c). The observed morphology is somewhat astonishing, as the pronounced terraces and the axial stacking in the present system are both energetically unfavorable. The first due to increased interface with water and the latter because of the non-selectivity of the CTAB surfactant. The use of one surfactant for the stabilisation of diblock copolymer droplets has typically resulted in concentric lamellae where one phase preferentially faces towards the interface. Axially stacked lamellae usually required two surfactants to enhance the compatibility of both polymer phases towards the high-energy polymer/water interface.[8, 32] We thus attribute this special microphase behaviour to the brush topology. During microphase separation in spherical confinement there are (at least) two competing forces at play: (i) in-plane packing of stretched brushes and (ii) preference of one block towards the interface. Whereas the first results in a planar arrangement and stacked disc (or lamella given a $f_A \sim 50$ wt%) formation, the latter would promote concentric lamellae where one block shares the interface with CTAB/water. The strong tendency of polymer brushes with stretched backbone for dense pack densely into planar layers favors low curvature disk formation over bending into high curvature concentric lamellae. Through axial stacking, the curvature remains low for all lamellae (discs); whereas in a concentric arrangement of lamellae (onion-like particle), the curvature – and thus energetic penalties from bending and splay – dramatically increase towards the particle centre. Since we exclusively find axial stacking of lamellae, the enthalpic gain of in-plane packing dominates the energetic penalty of unfavourable PLA/CTAB/water interface. On closer inspection of the TEM images, the system further minimises this penalty by reducing the PLA/CTAB/water interface through necking (Figure S8). PLA is evading into the

microparticle while the PS lamellae cover the particle surface almost completely. Overall, this unforeseen morphology demonstrates the necessity to investigate the self-assembly behavior of molecular brushes and other polymer topologies in confinement as deviations from the predicted nanostructures are to be expected.

3. Conclusions

We investigated the self-assembly of high molecular weight diblock MPBs in the spherical confinement of nanoemulsion droplets and found well-defined bi-continuous or axially-stacked lamellar morphologies defined by the PS/PLA block weight fraction. Our findings lay the foundation for future studies in targeting other classical morphologies known for diblock copolymers. Potential areas of application for internally structured particles are being actively investigated, including the incorporation of responsive features[32-35] as well as capture and release properties.[36, 37] Our findings also inspire more sophisticated self-assembly scenarios, such as assembling (polymer) Janus nanoparticles or (rod-like) diblock MPBs with intrinsic stiffness.[24] Similarly, high aspect ratio diblock MPBs may be used to considerably increase the periodicity of polymer domains,[26] leading to increased spacing between the stacked (or even concentric) lamellae.

Supporting Information

Supporting Information is available from the Wiley Online Library.

Acknowledgements: The authors made use of the facilities of the Imaging Centre Essen (IMCES) at the University Clinic in Essen. The authors thank A/Prof C. Neto for providing access to atomic force microscopes. A.S. is grateful to Evonik industries for a PhD fellowship. T.P. thanks the University of Sydney Nano Institute for a Postgraduate Top-Up Scholarship. M.M. acknowledges the Faculty of Science (University of Sydney) Seedfunding scheme and the Australian Research Council for a Discovery Early Career Researcher Award

(DE180100007). A.H.G. thanks Evonik industries for financial support through an endowed professorship (2016-2022) and the German Research Foundation (DFG) for funding an Emmy Noether Young Researcher Group (2017-2022; #376920678).

Keywords: controlled polymerisation; electron tomography; emulsions; microphase separation; polymer bottlebrushes

References

[1] F. H. Schacher, P. A. Rupar, I. Manners, *Angew. Chem. Int. Ed.* **2012**, *51*, 7898.
[2] A. H. Groschel, A. H. E. Muller, *Nanoscale* **2015**, *7*, 11841.
[3] C. M. Bates, F. S. Bates, *Macromolecules* **2017**, *50*, 3.
[4] J.-F. Lutz, J.-M. Lehn, E. W. Meijer, K. Matyjaszewski, *Nat. Rev. Mater.* **2016**, *1*, 16024.
[5] Y. Wu, G. Cheng, K. Katsov, S. W. Sides, J. Wang, J. Tang, G. H. Fredrickson, M. Moskovits, G. D. Stucky, *Nat. Mater.* **2004**, *3*, 816.
[6] H. Yabu, T. Jinno, K. Koike, T. Higuchi, M. Shimomura, *J. Polym. Sci. Part B: Polym. Phys.* **2011**, *49*, 1717.
[7] C. Chen, R. A. L. Wylie, D. Klinger, L. A. Connal, *Chem. Mater.* **2017**, *29*, 1918.
[8] S.-J. Jeon, G.-R. Yi, S.-M. Yang, *Adv. Mater.* **2008**, *20*, 4103.
[9] H. Yabu, T. Higuchi, H. Jinnai, *Soft Matter* **2014**, *10*, 2919.
[10] J. M. Shin, Y. Kim, H. Yun, G.-R. Yi, B. J. Kim, *ACS Nano* **2017**, *11*, 2133.
[11] S. G. Jang, D. J. Audus, D. Klinger, D. V. Krogstad, B. J. Kim, A. Cameron, S.-W. Kim, K. T. Delaney, S.-M. Hur, K. L. Killops, G. H. Fredrickson, E. J. Kramer, C. J. Hawker, *J. Am. Chem. Soc.* **2013**, *135*, 6649.
[12] D. Klinger, M. J. Robb, J. M. Spruell, N. A. Lynd, C. J. Hawker, L. A. Connal, *Polym. Chem.* **2013**, *4*, 5038.
[13] K. H. Ku, J. M. Shin, M. P. Kim, C.-H. Lee, M.-K. Seo, G.-R. Yi, S. G. Jang, B. J. Kim, *J. Am. Chem. Soc.* **2014**, *136*, 9982.
[14] B. V. K. J. Schmidt, J. Elbert, D. Scheid, C. J. Hawker, D. Klinger, M. Gallei, *ACS Macro Lett.* **2015**, *4*, 731.
[15] H. Yang, K. H. Ku, J. M. Shin, J. Lee, C. H. Park, H.-H. Cho, S. G. Jang, B. J. Kim, *Chem. Mater.* **2016**, *28*, 830.
[16] B. V. K. J. Schmidt, C. X. Wang, S. Kraemer, L. A. Connal, D. Klinger, *Polym. Chem.* **2018**.
[17] K. Zhang, L. Gao, Y. Chen, Z. Yang, *J. Colloid Interface Sci.* **2010**, *346*, 48.
[18] J. Xu, K. Wang, J. Li, H. Zhou, X. Xie, J. Zhu, *Macromolecules* **2015**, *48*, 2628.
[19] M. Müllner, *Macromol. Chem. Phys.* **2016**, *217*, 2209.
[20] M. Müllner, A. H. E. Müller, *Polymer* **2016**, *98*, 389.
[21] M. Zhang, A. H. E. Müller, *J. Polym. Sci. Part A: Polym. Chem.* **2005**, *43*, 3461.
[22] S. S. Sheiko, B. S. Sumerlin, K. Matyjaszewski, *Progr. Polym. Sci.* **2008**, *33*, 759.
[23] R. Verduzco, X. Li, S. L. Pesek, G. E. Stein, *Chem. Soc. Rev.* **2015**, *44*, 2405.
[24] T. Pelras, C. S. Mahon, M. Mullner, *Angew. Chem. Int. Ed.* **2018**.
[25] W. Gu, J. Huh, S. W. Hong, B. R. Sveinbjornsson, C. Park, R. H. Grubbs, T. P. Russell, *ACS Nano* **2013**, *7*, 2551.

[26] R. J. Macfarlane, B. Kim, B. Lee, R. A. Weitekamp, C. M. Bates, S. F. Lee, A. B. Chang, K. T. Delaney, G. H. Fredrickson, H. A. Atwater, R. H. Grubbs, *J. Am. Chem. Soc.* **2014**, *136*, 17374.
[27] Y. Xia, B. D. Olsen, J. A. Kornfield, R. H. Grubbs, *J. Am. Chem. Soc.* **2009**, *131*, 18525.
[28] J. Rzayev, *Macromolecules* **2009**, *42*, 2135.
[29] J. Bolton, T. S. Bailey, J. Rzayev, *Nano Lett.* **2011**, *11*, 998.
[30] M. W. Matsen, F. S. Bates, *Macromolecules* **1996**, *29*, 1091.
[31] A. S. Zalusky, R. Olayo-Valles, J. H. Wolf, M. A. Hillmyer, *J. Am. Chem. Soc.* **2002**, *124*, 12761.
[32] D. Klinger, C. X. Wang, L. A. Connal, D. J. Audus, S. G. Jang, S. Kraemer, K. L. Killops, G. H. Fredrickson, E. J. Kramer, C. J. Hawker, *Angew. Chem. Int. Ed.* **2014**, *53*, 7018.
[33] T. Higuchi, K. Motoyoshi, H. Sugimori, H. Jinnai, H. Yabu, M. Shimomura, *Macromol. Rapid Commun.* **2010**, *31*, 1773.
[34] R. Deng, F. Liang, W. Li, Z. Yang, J. Zhu, *Macromolecules* **2013**, *46*, 7012.
[35] J. Lee, K. H. Ku, M. Kim, J. M. Shin, J. Han, C. H. Park, G.-R. Yi, S. G. Jang, B. J. Kim, *Adv. Mater.* **2017**, *29*, 170068.
[36] H. Yu, X. Qiu, S. P. Nunes, K.-V. Peinemann, *Nat. Commun.* **2014**, *5*, 4110.
[37] Y. La, C. Park, T. J. Shin, S. H. Joo, S. Kang, K. T. Kim, *Nat. Chem.* **2014**, *6*, 534.

Diblock molecular polymer brushes self-assemble under confinement in drying emulsion droplets to form uniform microparticles with complex or highly ordered internal structure. Bi-continuous or axially-stacked lamellar morphologies can be accessed by altering the block ratio of the brush.

Andrea Steinhaus,[±] Théophile Pelras,[±] Ramzi Chakroun, André H. Gröschel,* Markus Müllner*

Self-assembly of diblock molecular polymer brushes in the spherical confinement of nanoemulsion droplets

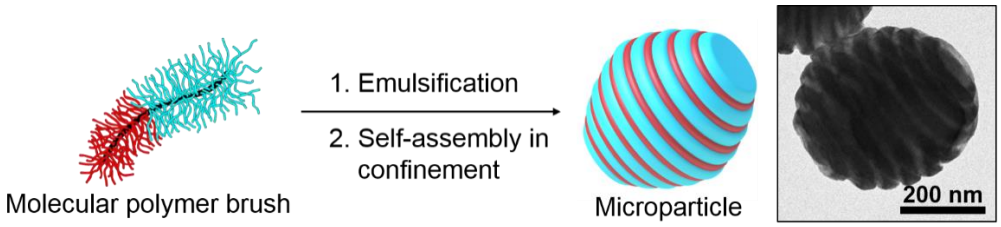

((Supporting Information should be included here for submission only; for publication, please provide Supporting Information as a separate PDF file.))

Supporting Information

for *Macromol. Rapid Commun.*, DOI: 10.1002/marc.2013#####

Self-assembly of diblock molecular polymer brushes in the spherical confinement of nanoemulsion droplets

Andrea Steinhaus,[±] Théophile Pelras,[±] Ramzi Chakroun, André H. Gröschel,[*] Markus Müllner[*]

[±]The authors contributed equally.

A. Steinhaus (M.Sc.), R. Chakroun (M.Sc.), Prof. Dr. A.H. Gröschel

Physical Chemistry and Center for Nanointegration Duisburg-Essen (CENIDE), University Duisburg-Essen, 47057 Duisburg, Germany.

E-mail: andre.groeschel@ude.de

T. Pelras (M.Sc.), Dr. M. Müllner

Key Centre for Polymers and Colloids, School of Chemistry, and The University of Sydney Nano Institute (Sydney Nano), The University of Sydney, Sydney 2006, New South Wales, Australia.

E-mail: markus.muellner@sydney.edu.au

MATERIALS

All chemicals were used as received unless stated otherwise. 4-Cyano-4-(thiobenzoylthio) pentanoic acid (CTBPA)[1] and *2*-(*2*-bromoisobutyryloxy)ethyl methacrylate (BIEM)[2] were synthesised according to published procedures. *2*-(trimethylsilyloxy)ethyl methacrylate (TMS-HEMA, 96%), *1,1,4,7,10,10*-hexamethyltriethylenetetramine (HMTETA, 97%), styrene (99%), *1,4*-dioxane (99%), cetrimonium bromide (CTAB, >99%), polyvinyl alcohol (PVA, M_n = 13-23 kg·mol^{-1}, 87-89%), sodium dodecyl sulfate (SDS, >99%) were received from Sigma-Aldrich. Copper(I) chloride (CuCl) and anisole (≥ 99 %) were obtained from Merck. *N,N*-dimethylformamide (DMF, 99.9%) was dried using an Innovative Technology Pure Solv apparatus. *1,8*-diazabicyclo[5.4.0]undec-*7*-ene (DBU, ≥99%) was obtained from Fluka. *L*-lactide (*L*-LA) was purchased from Alfa and recrystallized from ethyl acetate. Azobisisobutyronitrile (AIBN) was purchased from Condea Chemie and recrystallized from methanol. Deuterated chloroform ($CDCl_3$, 99%) and deuterated dimethyl sulfoxide (DMSO-d_6, 99%) were purchased from Cambridge Isotopes Laboratories, Inc. The methacrylic/vinylic monomers were passed through a short silica column to remove the inhibitor. Ultrapure water was obtained from a Milli-Q® Integral Water Purification System and used for the preparation of emulsions and purification. As dialysis tube a cellulose membrane was used with an average flat width of 33 mm and a MWCO of 12-14 kDa (Sigma Aldrich).

METHODS

Nuclear magnetic resonance (^{1}H NMR) spectra were recorded in deuterated solvents using a 300 MHz Bruker Avance system at 25 ºC. End-group analysis and/or monomer conversion were used to determine the degree of polymerisation and calculate the molecular weight. Gel permeation chromatography (GPC) measurements were performed on an UFLC Shimadzu Prominence GPC system running using DMAc/LiBr and a flow rate of 1 mL min^{-1} at 50 ºC. Samples (5 g·L^{-1}) were dissolved and pressed through a 222 nm PTFE filter prior to injection. Atomic force microscopy (AFM) imaging was performed in air using a Bruker Multimode-8 with tapping-mode cantilevers (48 Nm^{-1}, Tap190Al-G, Budget Sensors, Bulgaria). AFM specimen were prepared by drop-casting a solution of molecular polymer brushes (0.01 g·L^{-1}, in chloroform) on a freshly cleaved mica plate and subsequently dry-blowing using a stream of nitrogen. Images were processed with Bruker Nanoscope software. Dynamic light scattering (DLS) was conducted on a LS spectrometer operated with a HeNe laser (max. 100 mW constant power output at λ = 632.8 nm). Samples were prepared with concentrations of 0.1 g·L^{-1} and

purified from dust by passing through a PTFE filter of 5 µm pore size directly into dust-free cylindrical quartz cuvettes (diameter 10 mm). Three intensity-time autocorrelation functions were measured at a scattering angle of 90° with an acquisition time of 60 seconds. The recorded data was analysed with LS spectrometer v.63 software package. The transmission electron microscopy (TEM) measurements were performed on a JEOL JEM-1400 Plus TEM, operating at an accelerating voltage of 120 kV, a point resolution of 0.38 nm as well as a line resolution of 0.2 nm. Images were recorded with 16-bit 4096×4096 Pixel CMOS digital camera and processed FIJI open-source software package.[3] For sample preparation, one drop of the polymer brush dispersion (c = 0.1 g·L^{-1}) was deposited on a carbon-coated copper grid (200 mesh, Science Services) and excess solution was blotted after 30s using filter paper. All samples were stained with RuO_4 for 15 min prior to measurements.

The TEM tomography (ET) tilt series of microparticles were acquired between ±70° in 3° increments with the SerialEM software package (version 3.2.2). For image alignment purposes, the TEM grids were dipped in gold nanoparticle (fiducial markers) solution before sample deposition (d = 3–10 nm, stabilized by dodecane thiol ligand). Pre-alignment of tilt image series was done with IMOD.[4] Volumetric graphics and analyses were performed with the UCSF Chimera package[5] and low-pass filtered with Chimera's Gaussian filter with 3.0 voxel radius. The supporting video 1 was compiled after alignment using Fiji.

The scanning electron microscopy (SEM) measurements were performed on a cryo-field emission SEM equipped with in lens-, chamber- as well as energy-selective detectors for 16 Bit image series acquisition with up to 40,000×50,000-pixel resolution. Samples for SEM measurements were prepared by putting one drop of an approximately 0.1 g·L^{-1} sample dispersion on a mica wafer. After 30s the solution was blotted with a paper tissue and the wafer was dried for at least 12 h. Afterwards a layer of 2 nm was sputtered on the samples using a Quorum PP3010T-Cryo chamber with integrated Q150T-Es high-end sputter coater and Pt-Cd target.

EXPERIMENTAL SECTION

Synthesis of macro-CTA PBIEM$_{92}$. CTBPA (11.6 mg, 41.6 µmol), BIEM (1.98 g, 7.10 mmol), AIBN (2.6 mg, 15.9 µmol) and anisole (3 mL) were charged into a Schlenk flask and mixed thoroughly. The mixture was degassed via three freeze-pump-thaw cycles and the vessel was backfilled with nitrogen. The polymerisation was performed at 70 ºC for 6 hours and stopped by cooling and exposing the mixture to air. The polymer was precipitated in hexane

three times, dissolved in dioxane and freeze-dried overnight. The degree of polymerisation was determined using end-group analysis, comparing the CTA peak (2H, 7.8 ppm) and the PBIEM signal (2H, 4.2 ppm; 2H, 4.4 ppm). DP_{PBIEM} = 92, $M_{n,NMR}$ = 25.7 kg·mol^{-1}, Đ = 1.11.

Synthesis of PBIEM$_{92}$-*b*-P(TMS-HEMA)$_{104}$. PBIEM$_{92}$-CTA (102 mg, 3.97 μmol), TMS-HEMA (315 mg, 1.56 mmol), AIBN (0.16 mg, 0.97 μmol) and dioxane (1.2 mL) were charged into a Schlenk flask and mixed thoroughly. The blend was degassed via three freeze-pump-thaw cycles and the vessel was backfilled with nitrogen. The polymerisation was performed at 70 ºC for 6 hours and stopped by cooling and exposing the mixture to air. The polymer was precipitated in hexane once, dissolved in dioxane and freeze-dried overnight. The degree of polymerisation was determined using end-group analysis, comparing the PBIEM peaks (2H, 4.2 ppm; 2H, 4.4 ppm) and the P(TMS-HEMA) signal (2H, 3.8 ppm; 2H, 4.0 ppm) $DP_{TMS-PHEMA}$ = 104, $M_{n,NMR}$ (diblock) = 46.7 kg·mol^{-1}, Đ = 1.22.

Synthesis of PBIEM$_{92}$-*b*-PHEMA$_{104}$. The trimethylsilyl groups were removed by dissolving 100 mg of the PBIEM$_{92}$-*b*-P(TMS-HEMA)$_{104}$ in methanol with acetic acid (10 v/v%) and stirring for 24 hours. The deprotected polymer was dialysed in acetone overnight, evaporated at reduced pressure, redissolved in dioxane and freeze-dried overnight. ^{1}H NMR confirmed ≥99 % TMS removal resulting in PBIEM$_{92}$-*b*-PHEMA$_{104}$. $M_{n,NMR}$ (diblock) = 39.5 kg·mol^{-1}, Đ = 1.32.

Synthesis of PBIEM$_{92}$-*b*-[PHEMA$_{104}$-*g*-PLA$_{33}$]. PBIEM$_{92}$-*b*-PHEMA$_{104}$ (30 mg, 10.4 mg HEMA, 80.0 μmol HEMA), *L*-LA (342 mg, 2.38 mmol) and dry DMF (2 mL) were charged into a dry round bottom flask and stirred thoroughly. DBU (12.2 mg, 80.0 μmol) was added and the vessel was sealed with a glass stopper. The reaction was performed for 2.5 hours and the mixture was transferred into a dialysis membrane (14 kDa cut-off) and dialysed overnight. Fractionated precipitation in THF using hexane was preformed to remove linear PLA (initiated from traces of water). The polymer was concentrated under reduced pressure, dissolved in dioxane and freeze-dried overnight. The ratio of the PBIEM peak (6H, 1.9 ppm) and the PLA peak (1H, 5.1 ppm) was used to calculate the PLA brush. DP_{PLA} = 33, $M_{n,NMR}$ (tad-pole MPB) = 286 kg·mol^{-1}.

Synthesis of [PBIEM$_{92}$-*g*-PS$_{25}$]-*b*-[PHEMA$_{104}$-*g*-PLA$_{24}$]. PBIEM$_{92}$-*b*-[PHEMA$_{104}$-*g*-PLA$_{33}$] (30 mg, 3.39 mg BIEM, 12.2 μmol BIEM), S (504 mg, 4.85 mmol), HMTETA (2.8 mg, 12 μmol) and anisole (2.8 mL) were charged into a Schlenk flask and stirred thoroughly. The

mixture was degassed via three freeze-pump-thaw cycles, CuCl (1.2 mg, 12 μmol) was added onto the frozen mixture, the vessel was degassed again and backfilled with nitrogen. The polymerization was performed at 100 ºC for 2 hours and stopped by cooling and exposing the mixture to air. The polymer was precipitated in cold hexane and dialysed in acetone overnight. The diblock MPBs were stored in acetone solution until further use. The ratio of PLA peak (1H, 5.1 ppm) and the PS peak (2H, 6.5 ppm) was used to calculate the PS brush, assuming all initiation sites have been grafted equally. DP_{PS} = 6 (MPB1) and 24 (MPB2), $M_{n,NMR}$ (diblock MPB) = 343 kg·mol^{-1} (MPB1) and 516 kg·mol^{-1} (MPB2).

Preparation of emulsion droplets. For the following preparation an aqueous stock solution of CTAB (c = 10 g·L^{-1}) was prepared by dissolving the surfactant in Millipore water while heating. Exemplified on MPB1, in a 5 mL glass vial, 2 mL of CTAB solution was added to 150 μL of $CHCl_3$ solution with a MPB1 concentration of c = 6.67 g·L^{-1}. For emulsification the mixture was vortexed for 1 min and $CHCl_3$ was evaporated at room temperature in open vials for 5 days under continuous stirring. To remove excess CTAB the droplet emulsion was purified by dialysis. Samples with the other surfactants (SDS and PVA) were prepared following the same procedure.

SUPPORTING FIGURES

S1 Proton Nuclear Magnetic Resonance of diblock brush synthesis steps

^{1}H NMR of PBIEM$_{92}$

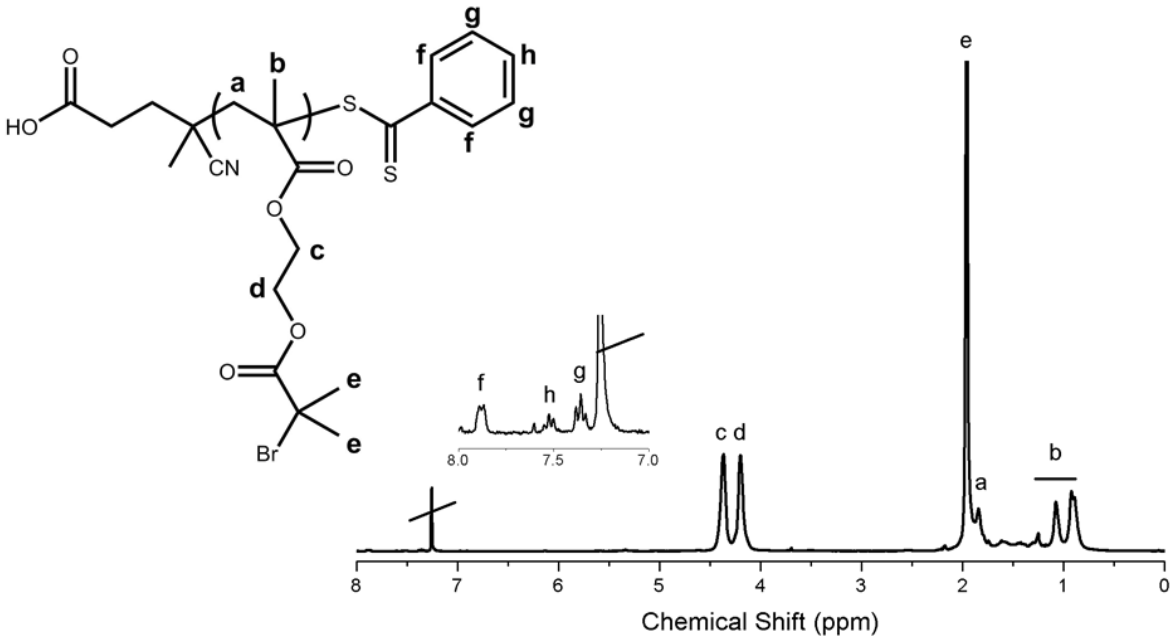

Figure S1-1: ^{1}H NMR spectrum of PBIEM$_{92}$ in $CDCl_3$.

^{1}H NMR of PBIEM$_{92}$-*b*-P(TMS-HEMA)$_{104}$

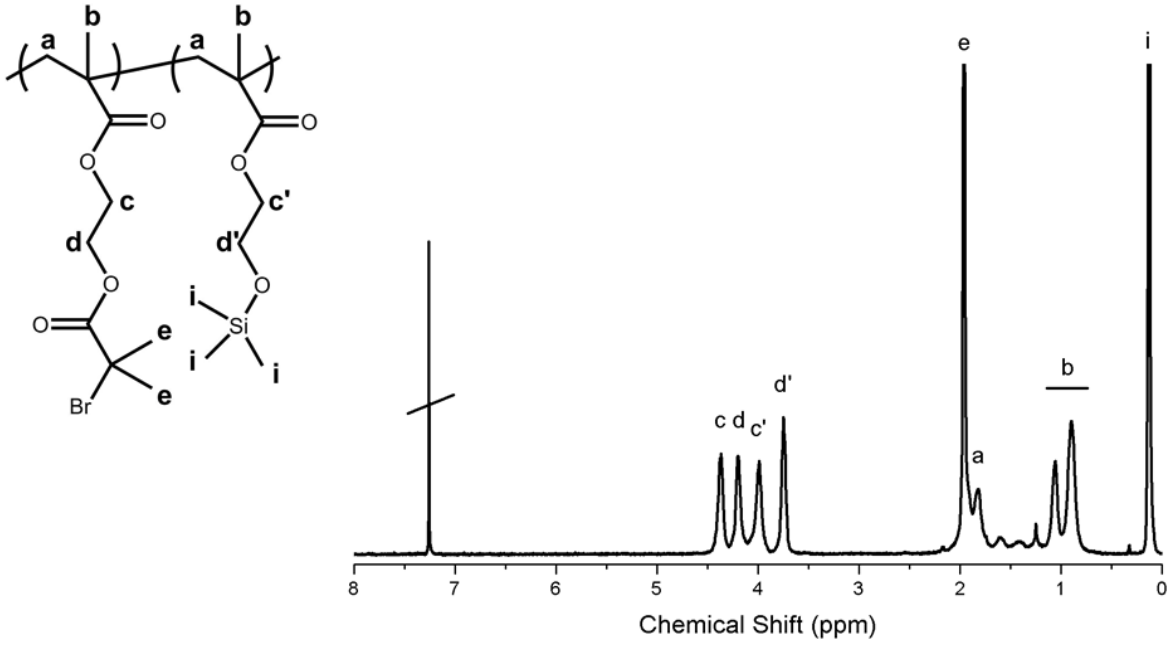

Figure S1-2: ^{1}H NMR spectrum of PBIEM$_{92}$-*b*-P(TMS-HEMA)$_{104}$ in $CDCl_3$.

^{1}H NMR of PBIEM$_{92}$-b-PHEMA$_{104}$

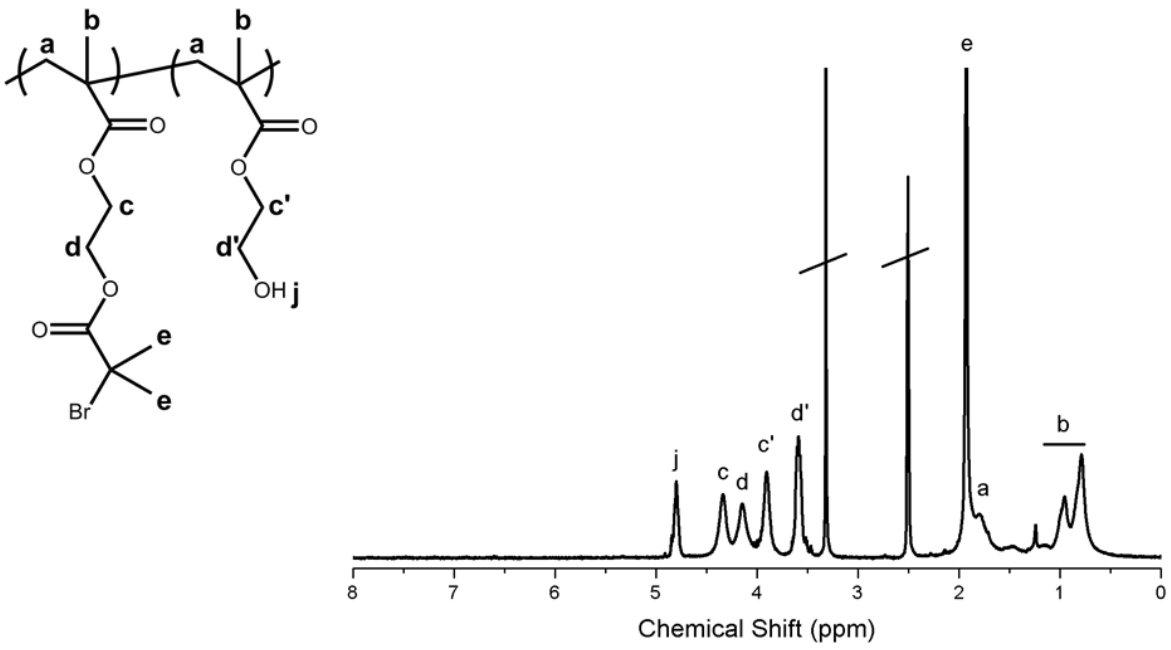

Figure S1-3: ^{1}H NMR spectrum of PBIEM$_{92}$-*b*-PHEMA$_{104}$ in DMSO-d$_6$.

^{1}H NMR of PBIEM$_{92}$-*b*-[PHEMA$_{104}$-*g*-PLA$_{33}$]

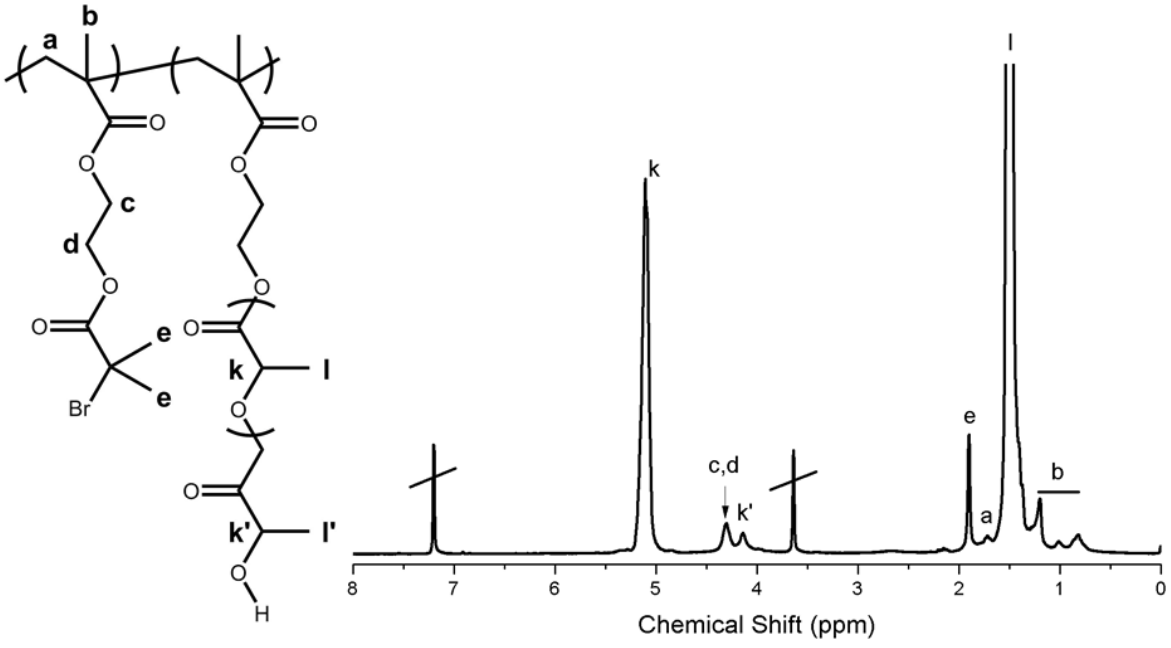

Figure S1-4: ^{1}H NMR spectrum of PBIEM$_{92}$-*b*-[PHEMA$_{104}$-*g*-PLA$_{33}$] in CDCl$_3$.

^{1}H NMR of [PBIEM$_{92}$-*g*-PS$_{6}$]-*b*-[PHEMA$_{104}$-*g*-PLA$_{33}$] (MPB1)

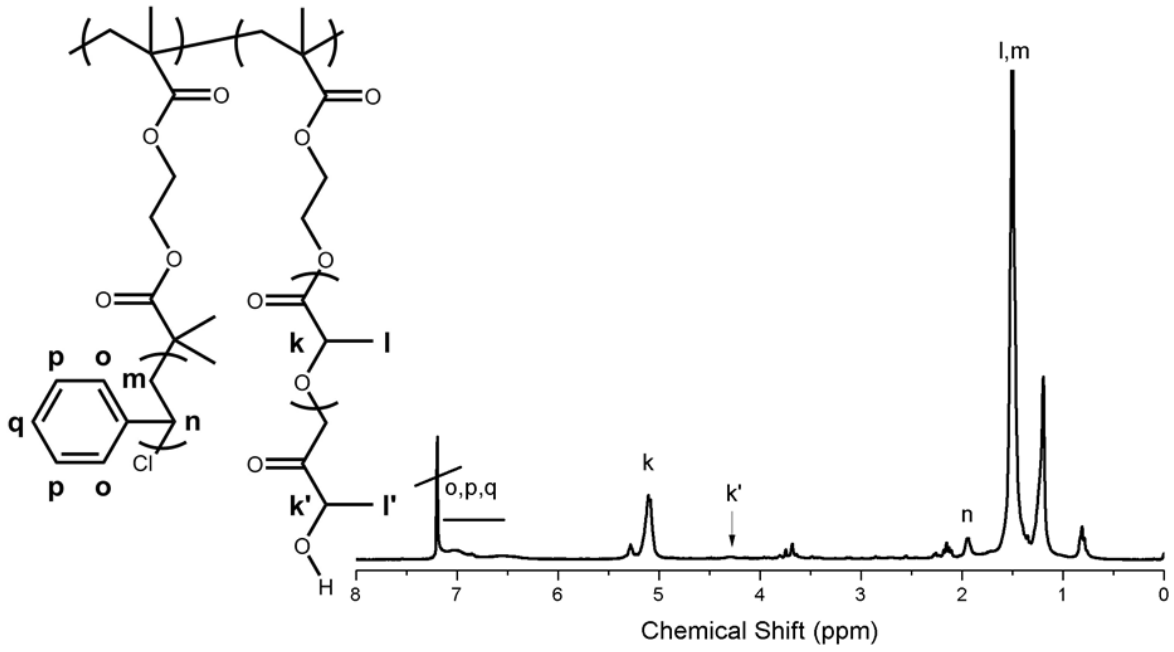

Figure S1-6: ^{1}H NMR spectrum of [PBIEM$_{92}$-*g*-PS$_{6}$]-*b*-[PHEMA$_{104}$-*g*-PLA$_{33}$] in $CDCl_3$.

^{1}H NMR of [PBIEM$_{92}$-*g*-PS$_{24}$]-*b*-[PHEMA$_{104}$-*g*-PLA$_{33}$] (MPB2)

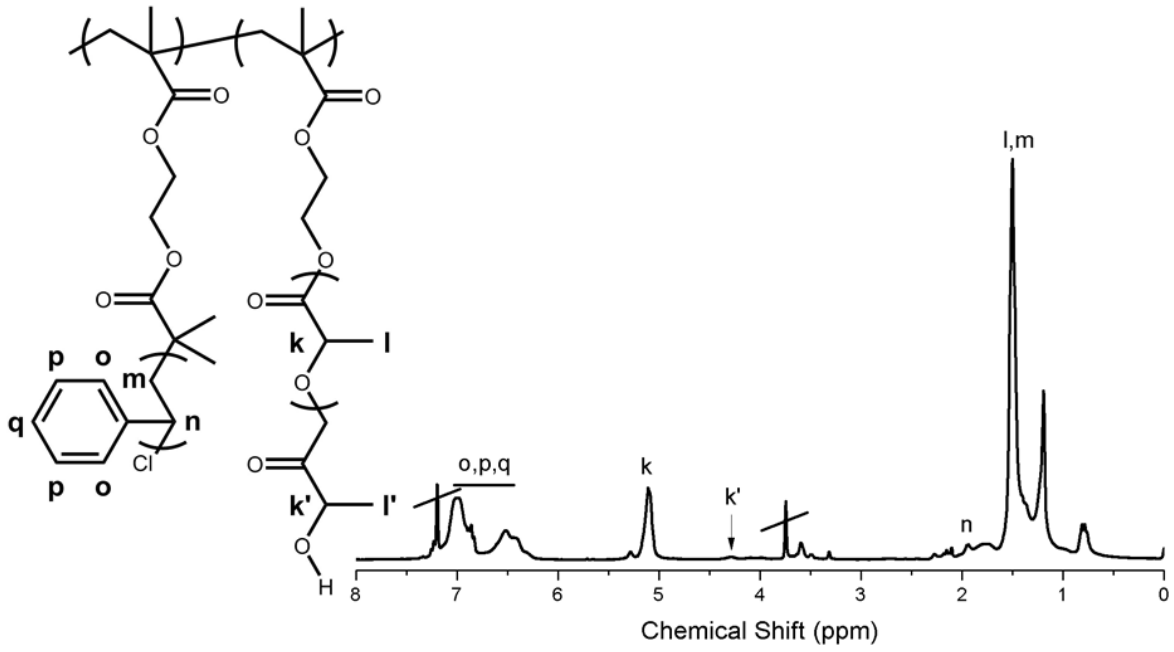

Figure S1-6: ^{1}H NMR spectrum of [PBIEM$_{92}$-*g*-PS$_{24}$]-*b*-[PHEMA$_{104}$-*g*-PLA$_{33}$] in $CDCl_3$.

S2 Atomic Force Microscopy on the MPBs

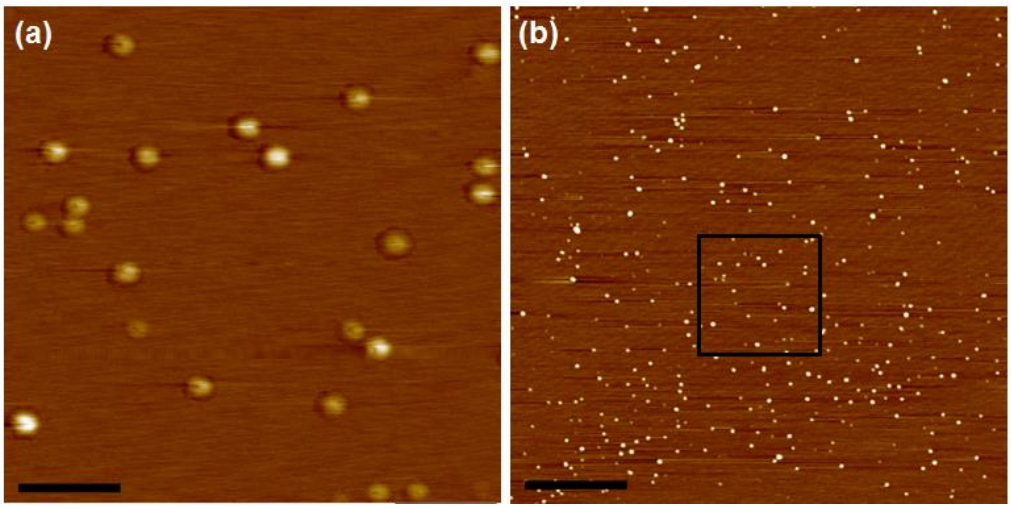

Figure S2-1. AFM of MPB1 drop-cast (0.01 $g \cdot L^{-1}$ in chloroform) onto freshly-cleaved mica. Scale bars are 200 nm for (a) and 1000 nm for (b). Z-scale is ±10 nm for all images.

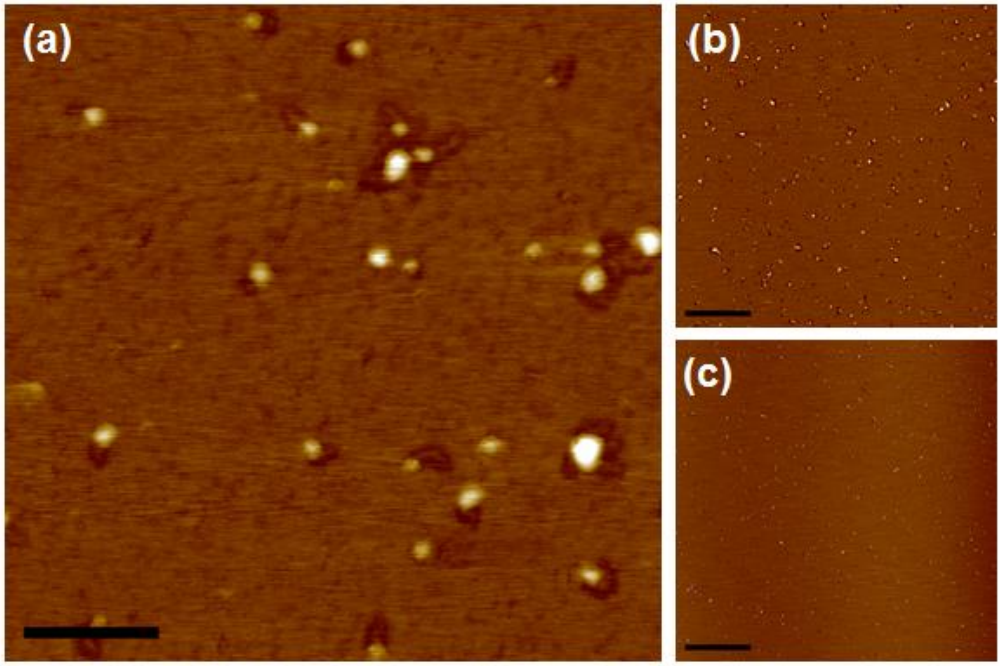

Figure S2-2. AFM of MPB2 drop-cast from chloroform onto freshly-cleaved mica. Scale bars are 200 nm for (a), 1000 nm for (b) and 2000 nm for (c). Z-scale is ±10 nm for all images.

S3 Formation of microparticles using different surfactants

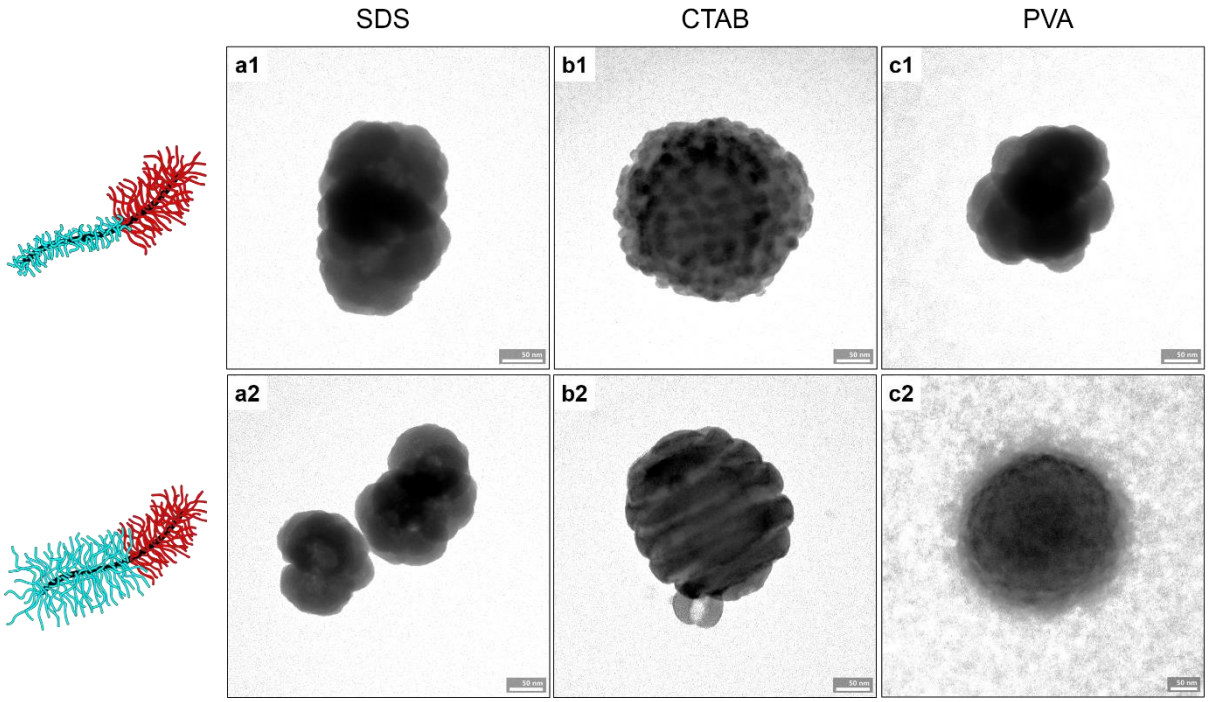

Figure S3. TEM images of individual microparticles prepared using different surfactants. The surfactants were (a) SDS, (b) CTAB, and (c) PVA. Scale bars are all 50 nm.

S4 Microparticles after acidic hydrolysis

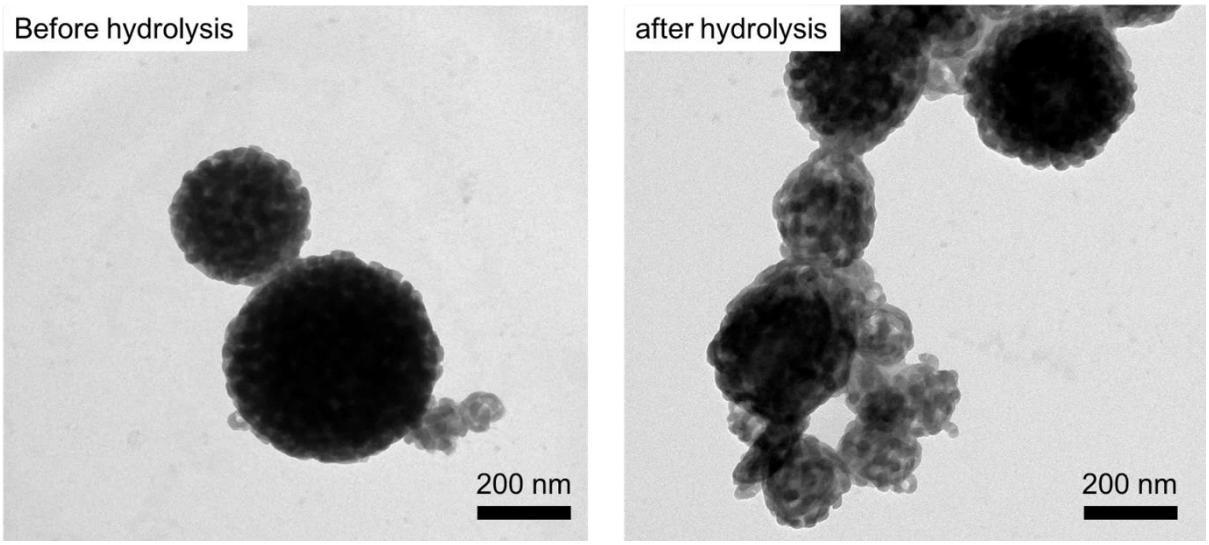

Figure S4: TEM images of MPB1 microparticles prepared with CTAB before (a) and after hydrolysis (b).

S5 Formation of microparticles using brushes with increasing PS content

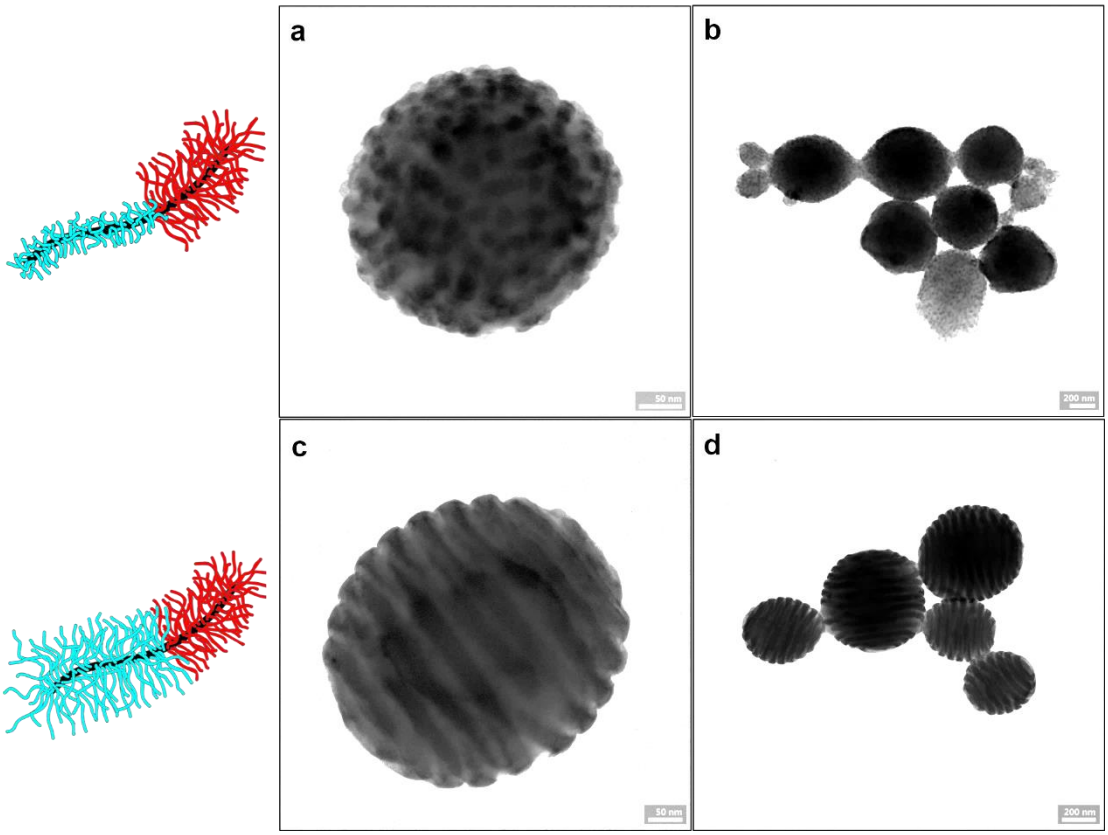

Figure S5: TEM images of individual microparticles prepared from MPB1 (a/b) and MPB2 (c/d) using CTAB as surfactant. Scale bars are 50 nm (a/b) and 200 nm (c/d).

S6 Grey-scale analysis of lamellar microparticles

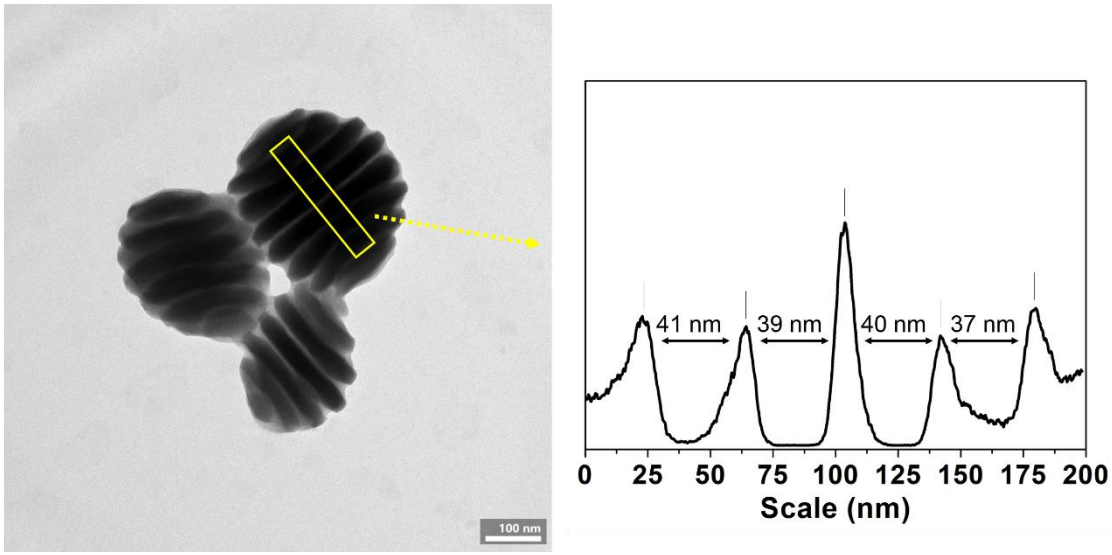

Figure S6: TEM image of MPB2-based microparticles and corresponding grey scale analysis of the lamellar structure of a particle laying on its long axis.

S7 Differential Scanning Calorimetry analysis

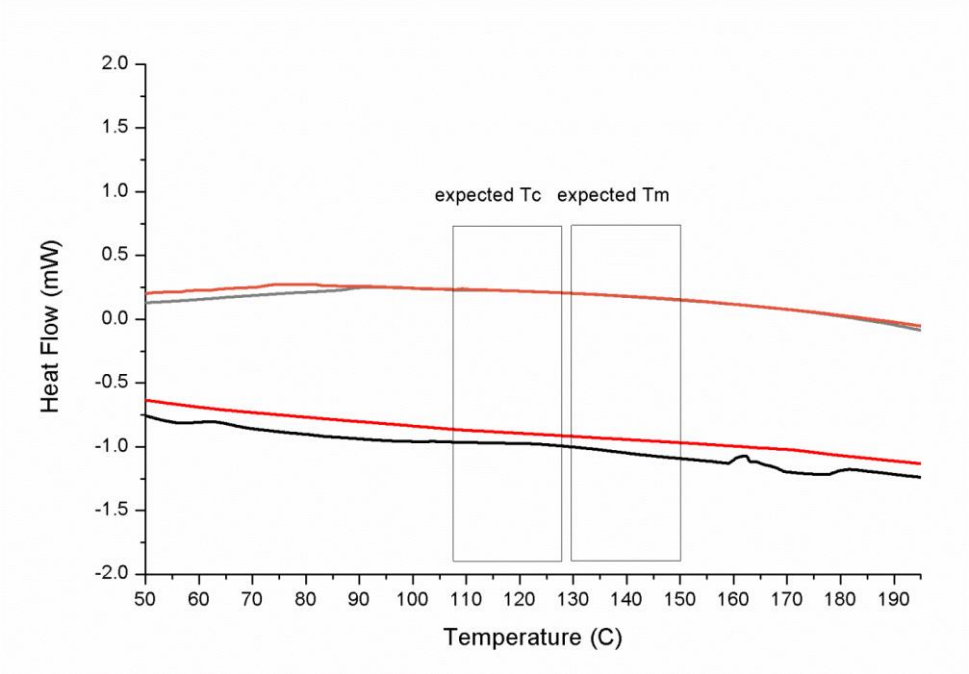

Figure S7: DSC analysis of the PBIEM$_{92}$-*b*-(PHEMA$_{104}$-*g*-PLA$_{33}$) revealing the absence of the expected crystallisation and melting temperatures for *L*-PLA. First heating (bottom, black) cooling (top, grey) cycle. Second heating (bottom, red) and cooling (top, orange) cycle.

S8 Minimisation of the PLA interface

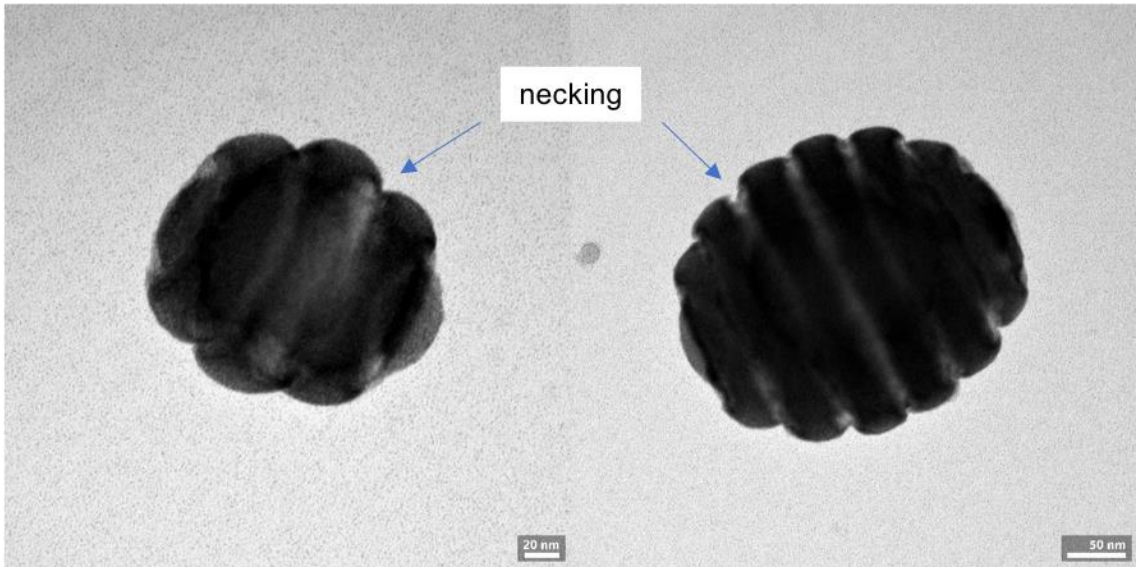

Figure S8: The unfavourable PLA/CTAB/water interface leads to the contraction of the PLA phase and its evasion into the particle, noticeable as necking.

SUPPORTING REFERENCES

[1] Thang, S. H.; Chong, (Bill)Y.K.; Mayadunne, R. T. A.; Moad, G.; Rizzardo, E. *Tetrahedron Lett.* **1999**, *40*, 2435.
[2] Matyjaszewski, K.; Gaynor, S. G.; Kulfan, A.; Podwika, M. *Macromolecules* **1997**, *30*, 5192.
[3] Schindelin, J.; et al. *Nat. Methods* **2012**, *9*, 676.
[4] Kremer, J. R.; Mastronarde, D. N.; McIntosh, J. R. *J. Struct. Biol.* **1996**, *116*, 71.
[5] Pettersen, E. F.; Goddard, T. D.; Huang, C. C.; Couch, G. S.; Greenblatt, D. M.; Meng, E. C.; Ferrin, T. E. *J. Comput. Chem.* **2004**, *25*, 1605.